A&A 382, 397–411 (2002)
DOI: 10.1051/0004-6361:20011534

Astronomy & Astrophysics

The cosmological constant and quintessence from a correlation function comoving fine feature in the 2dF quasar redshift survey

B. F. Roukema[1,2,3], G. A. Mamon[4,5], and S. Bajtlik[6]

[1] Inter-University Centre for Astronomy and Astrophysics, Post Bag 4, Ganeshkhind, Pune 411 007, India
[2] DARC/LUTH, Observatoire de Paris–Meudon, 5 place Jules Janssen, 92195 Meudon Cedex, France
[3] University of Warsaw, Krakowskie Przedmieście 26/28, 00-927 Warsaw, Poland
[4] Institut d'Astrophysique de Paris (CNRS UPR 341), 98bis Bd. Arago, 75014 Paris, France
e-mail: gam@iap.fr
[5] DAEC (CNRS UMR 8631), Observatoire de Paris-Meudon, 5 place Jules Janssen, 92195 Meudon Cedex, France
[6] Nicolaus Copernicus Astronomical Center, ul. Bartycka 18, 00-716 Warsaw, Poland
e-mail: bajtlik@camk.edu.pl

Received 20 June 2001 / Accepted 29 October 2001

Abstract. Local maxima at characteristic comoving scales have previously been claimed to exist in the density perturbation spectrum at the wavenumber $k = 2\pi/L_{\rm LSS}$, where $L_{\rm LSS} \sim 100$–$200\,h^{-1}$ Mpc (comoving), at low redshift ($z \lesssim 0.4$) for several classes of tracer objects, at $z \approx 2$ among quasars, and at $z \approx 3$ among Lyman break galaxies. Here, this cosmic standard ruler is sought in the "10K" initial release of the 2dF QSO Redshift Survey (2QZ–10K), by estimating the spatial two-point autocorrelation functions $\xi(r)$ of the three-dimensional (comoving, spatial) distribution of the $N = 2378$ quasars in the most completely observed and "covered" sky regions of the catalogue, over the redshift ranges $0.6 < z < 1.1$ ("low-z"), $1.1 < z < 1.6$ ("med-z") and $1.6 < z < 2.2$ ("hi-z"). Because of the selection method of the survey and sparsity of the data, the analysis was done conservatively to avoid non-cosmological artefacts. (i) Avoiding a priori estimates of the length scales of features, local maxima in $\xi(r)$ are found in all three different redshift ranges. The requirement that a local maximum be present in all three redshift ranges at a fixed comoving length scale implies strong, purely geometric constraints on the local cosmological parameters, in which case the length scale of the local maximum common to the three redshift ranges is $2L_{\rm LSS} = 244 \pm 17\,h^{-1}$ Mpc. (ii) For a standard cosmological constant FLRW model, the matter density and cosmological constant are constrained to $\Omega_{\rm m} = 0.25 \pm 0.10, \Omega_\Lambda = 0.65 \pm 0.25$ (68% confidence), $\Omega_{\rm m} = 0.25 \pm 0.15, \Omega_\Lambda = 0.60 \pm 0.35$ (95% confidence), respectively, *from the 2QZ–10K alone*. Independently of the type Ia supernovae data, the zero cosmological constant model ($\Omega_\Lambda = 0$) is rejected at the 99.7% confidence level. (iii) For an effective quintessence ($w_{\rm Q}$) model and zero curvature, $w_{\rm Q} < -0.5$ (68% confidence), $w_{\rm Q} < -0.35$ (95% confidence) are found, again *from the 2QZ–10K alone*. In a different analysis of a larger (but less complete) subset of the same 2QZ–10K catalogue, Hoyle et al. (2001) found a local maximum in the power spectrum to exist for widely differing choices of $\Omega_{\rm m}$ and Ω_Λ, which is difficult to understand for a genuine large scale feature at fixed comoving length scale. A resolution of this problem and definitive results should come from the full 2QZ, which should clearly provide even more impressive constraints on fine features in density perturbation statistics, and on the local cosmological parameters $\Omega_{\rm m}$, Ω_Λ and $w_{\rm Q}$.

Key words. cosmology: observations – cosmology: theory – distance scale – quasars: general – large-scale structure of Universe – reference systems

1. Introduction

Increasing observational evidence is mounting in favour of fine structure (local maxima) in the power spectrum or correlation function of the spatial distribution of extragalactic objects, at scales $\sim$100–$200\,h^{-1}$ Mpc. At redshifts $z \sim 2$–3, these features have been found among quasars and Lyman break galaxies (Deng et al. 1994; Broadhurst & Jaffe 1999; Roukema & Mamon 2000, 2001), and among low redshift objects, similar features have been found by numerous groups (e.g. Broadhurst et al. 1990; Broadhurst 1999; da Costa 1992; da Costa et al. 1993; Baugh & Efstathiou 1993, 1994; Gaztañaga & Baugh 1998; Einasto et al. 1994, 1997a,b; Deng et al. 1996; Tago et al. 2001; see Guzzo 1999 for a recent review, or Kirilova & Chizhov 2000 for a very extensive reference list).

Send offprint requests to: B. F. Roukema,
e-mail: boud.roukema@obspm.fr

Because the scale $\sim$100–200 h^{-1} Mpc is well into the linear regime of density perturbations and well above the present-day turnaround scale at which matter has had the time to collapse by self-gravity, *these features should occur at fixed comoving length scales*, provided that the correct values of the local cosmological parameters $\Omega_{\rm m}$ (the matter density parameter), Ω_Λ (the dimensionless cosmological constant) and $w_{\rm Q}$ (the effective quintessence parameter, e.g. Efstathiou 1999) are used to convert redshifts and angular positions to three-dimensional positions in three-dimensional (proper distance, comoving) space of the appropriate curvature (e.g. Roukema 2001).

At low redshifts ($z \lesssim 0.1$), peculiar velocities and the use of incorrect values of the local cosmological parameters make claims either for or against these fine features difficult. On the other hand, at high redshifts ($1 \lesssim z \lesssim 3$), while peculiar velocities have a much smaller effect and assumptions on the local cosmological parameters are more often stated clearly than for low redshift analyses, the main difficulty is the sparsity of observational data in homogeneous and large volume catalogues.

In Roukema & Mamon (2000, 2001), the objective prism survey of quasar candidates by Iovino et al. (1996) was analysed, using the a priori claim, primarily from the low redshift analyses, that a local maximum in the power spectrum or the spatial correlation function exists at $k = 2\pi/L_{\rm LSS}$, where $L_{\rm LSS} = 130 \pm 10\,h^{-1}$ Mpc. In a Fourier analysis of the initial release of data from the 2dF Quasar Survey (hereafter, 2QZ–10K, Croom et al. 2001), Hoyle et al. (2001) claim marginal evidence for the existence of a "spike" at 65–90 h^{-1} Mpc, depending on the values of the local cosmological parameters.

Spectroscopic followup of a small part of the Iovino et al. (1996) survey (P. Petitjean, private communication) suggests that it suffers from contamination by stars and by quasars at redshifts other than those estimated by Iovino et al. (1996), so it is possible that the features found were either underestimated or overestimated in strength and/or shifted in length scale with respect to the true signal.

On the contrary, the 2QZ–10K consists uniquely of diffraction grating spectroscopic redshifts, so should be free of this contamination and potentially provide a cleaner signal.

However, extreme care is required in the analysis of the 2QZ–10K survey, because of:

(a) the "angular selection function", i.e. the very anisotropic distribution of this initial release within the two survey regions (e.g. Fig. 1, Croom et al. 2001);
(b) the two sources of incompleteness in the regions observed so far: "spectroscopic incompleteness" (fraction of objects observed but with unsuccessful spectroscopic identification) and "coverage incompleteness" (fraction of target objects in a given field not yet spectroscopically observed); and
(c) the initial selection of the target catalogue using ub_Jr multi-colour photometry using photographic plates.

In this paper, a spatial correlation function analysis of the 2QZ–10K is performed, as in Roukema & Mamon (2001), in order to minimise spurious artefacts from factors (a)–(c) and enable a "comoving standard ruler" analysis of the data. Moreover, in order to avoid the a priori assumption of the scale at which feature(s) defining the standard ruler should occur, the constraint is relaxed to only require *consistency* of the scales of feature(s) between different redshift intervals of the 2QZ–10K, without assuming the scale(s) at which these feature(s) occur.

As will be seen below, consistency of length scales in the comoving spatial correlation function between different redshifts implies constraints on the local cosmological parameters *independently of cosmic microwave background, type Ia supernovae, or other constraints on these parameters*.

The observational catalogue and method of analysing it in a way that deals with points (a)–(c) above are briefly described in Sect. 2, results are presented in Sect. 3, the question of whether or not the comoving local maximum detected is a genuine, cosmological feature rather than just a noise fluctuation is discussed in Sect. 4 and conclusions are presented in Sect. 5.

An almost (i.e. perturbed) Friedmann-Lemaître-Robertson-Walker cosmological model is assumed here, optionally including a quintessence relation. The Hubble constant is parametrised as $h \equiv H_0/100\,{\rm km\ s^{-1}\ Mpc^{-1}}$. Comoving coordinates are used throughout (i.e. "proper distances", Eq. (14.2.21), Weinberg 1972, equivalent to "conformal time" if $c = 1$; see Roukema 2001 for a self-contained and conceptually simple presentation of how to calculate three-dimensional comoving separations for a curved space, by considering these as arc-lengths in four-dimensional space). Values of the density parameter, $\Omega_{\rm m}$, and the dimensionless cosmological constant, Ω_λ, are indicated where used.

For convenience, the reader is reminded here of the dependence of proper distance on $\Omega_{\rm m}$ and Ω_Λ, i.e.

$$\mathrm{d}(z) = \frac{c}{H_0} \int_{1/(1+z)}^{1} \frac{\mathrm{d}a}{a\sqrt{\Omega_{\rm m}/a - \Omega_\kappa + \Omega_\Lambda a^2}}, \qquad (1)$$

where a is the scale factor,

$$\Omega_\kappa \equiv \Omega_{\rm m} + \Omega_\Lambda - 1 \qquad (2)$$

is the (dimensionless) curvature of the observational Universe and

$$R_C \equiv \frac{c}{H_0} \frac{1}{\sqrt{|\Omega_\kappa|}} \qquad (3)$$

is its curvature radius.

Effective quintessence distance-redshift relations in a flat universe are also considered, where $\Omega_{\rm Q} \equiv 1 - \Omega_{\rm m}$ and $\Omega_{\rm Q} a^{-3(1+w_{\rm Q})}$ is substituted for Ω_Λ in Eq. (1), where $w_{\rm Q}$ is considered to be a constant (e.g. Efstathiou 1999). The value $w_{\rm Q} = -1$ corresponds to a standard cosmological constant metric.

Table 1. Angular subsamples of the 2QZ–10K survey. Listed are limits in right ascension (α_i) and declination (δ_i) in coordinate degrees; right ascension interval size θ in great circle degrees; approximate solid angle $\mathrm{d}\omega$ in square degrees; number of objects N; and a rough lower bound to the solid angular number density n in units of (sq. deg.)$^{-1}$. Note that the survey is not uniformly complete within these boundaries; completeness is modelled in the analysis by use of the angular positions of the observed quasars. This is why the number density estimates are only lower estimates.

# :	α_1	α_2	δ_1	δ_2	θ	$\mathrm{d}\omega$	N	n
1	147	155	−3	3	8.0	48.0	281	5.9
2	203	216	−3	1	13.0	52.0	323	6.2
3	−35	−30	−33	−28	5.0	21.6	194	9.0
4	−17	−2.5	−33	−27	14.5	75.3	681	9.0
5	21	31	−33	−27	10.0	51.9	364	7.0
6	40	50	−33	−27	10.0	51.9	535	10.3
total						300.7	2378	

2. Catalogue and analysis

2.1. The 2QZ

The 2QZ–10K is described in Croom et al. (2001). This release only includes quasars in regions of 85% or greater "spectroscopic completeness".

In order to minimise noise generated by "coverage incompleteness", only those quasars observed in regions with at least 80% coverage are included in the present analysis. The six highest solid angular density regions are chosen from Fig. 1 of Croom et al. (2001) and listed in Table 1, providing six independent sub-samples from which to obtain estimates of $\xi(r)$.

Together, these completeness criteria imply a minimum of about 70% total completeness, apart from the incompleteness implied by initial selection of target objects using photographic ub_Jr photometry (as opposed to spectroscopic observation of *all* objects, selected in a single filter from CCD photometry).

In Roukema & Mamon (2000, 2001), the high number density, objective prism survey near the South Galactic Pole (Iovino et al. 1996) was analysed. The right ascension and declination subsamples of the survey in the Roukema & Mamon (2001) analysis had solid angular number densities of 9.8 and 8.8 quasars/sq.deg. respectively.

The regions of the 2QZ so far completed have solid angular number densities similar to this (lower bounds are listed in Table 1), but since a larger redshift interval is covered, the comoving spatial densities are about a factor of three lower. The signal-to-noise ratios of a peak (local maximum) in $\xi(r)$ may not be as high in the 2QZ as in the Iovino et al. (1996) survey. Note that the two surveys are independent in angular and redshift range, apart from a slight overlap.

2.2. Method

2.2.1. Calculation of correlation functions

The correlation functions are calculated in three-dimensional curved space via $\xi(r) = (DD - 2DR/n + RR/n^2)/(RR/n^2)$ where DD, DR and RR indicate numbers of data-data, data-random and random-random quasar pairs respectively (Landy & Szalay 1993), and $n = 20$ times more random points than data points are used. The random catalogues use (i) the exact set of angular positions of the catalogue quasars, and (ii) random permutations ("z scrambles", Sect. IIIb in Osmer 1981) of the observational set of redshifts. Bin size is $\Delta r = 5\,h^{-1}\,\mathrm{Mpc}$.

In each of the approximately equal redshift intervals $0.6 < z < 1.1$ ("low-z"), $1.1 < z < 1.6$ ("med-z") and $1.6 < z < 2.2$ ("hi-z"), $\xi(r)$ is calculated for each of the six angular sub-samples defined in Table 1.

Within each redshift interval, mean values of $\xi(r)$ and standard errors in the mean of $\xi(r)$ across the six subsamples are calculated, since these are independent subsamples. Each function ξ is smoothed by a Gaussian with $\sigma = 15\,h^{-1}\,\mathrm{Mpc}$. Weighting in inverse proportion to the number of pairs in each angular sub-sample is applied in order to obtain signal in proportion to the respective numbers of pairs.

2.2.2. Consistency of spikes at all redshifts

Although $L_{\mathrm{LSS}} \approx 130 \pm 10\,h^{-1}\,\mathrm{Mpc}$ has been claimed by several authors to be the scale of a local maximum in the power spectrum or correlation function, this is *not assumed* here.

Spikes are detected here as the first local maximum in $\xi(r)$ above a given minimum separation r_{min}, where $r_{\mathrm{min}} = 100, 150$ or $200\,h^{-1}\,\mathrm{Mpc}$. In order for the maxima not to be *too* local (e.g. a slightly high value in one bin at r surrounded by slightly lower values in immediately adjacent bins at $r - \Delta r$ and $r + \Delta r$), a smoothing by a Gaussian of width $\sigma = 15\,h^{-1}\,\mathrm{Mpc}$ is applied when searching for a local maximum.

For a local maximum to be considered detected and useful for constraining local cosmological parameters, the estimates of its position r^i_{max} should be consistent in all three redshift ranges. Quantitatively, this consistency is defined by requiring the values of r^i_{max} to agree within $\Delta r = 5\,h^{-1}\,\mathrm{Mpc}$ between the low-z and the med-z subsamples, and within $\Delta r = 5\,h^{-1}\,\mathrm{Mpc}$ between the med-z and the hi-z sub-samples, assuming Gaussian errors.

So, for a given value of r_{min}, the consistency hypothesis implies rejection probabilities P and confidence levels $1 - P$.

The above test is applied without any criteria regarding the significance of individual maxima, in order to be as parameter-free as possible, though at the risk of including noise.

For the sake of discussion, an estimate of the signal-to-noise ratio of a local maximum can be quantified as follows.

For a maximum at $r^i_{\rm max}$, define ξ^r, ξ_- and ξ_+ as the value of ξ at $r^i_{\rm max}$ and the values of ξ at the first minima at r_- and r_+ below and above $r^i_{\rm max}$ respectively, and take the root mean square value of $\sigma_{\langle\xi\rangle}(r)$ for $r \in [r_-, r_+]$. Then,

$$(S/N) \equiv \frac{\xi^r - (\xi_- + \xi_+)/2}{\sqrt{\left\langle \sigma^2_{\langle\xi\rangle}(r) \right\rangle}} \quad (4)$$

is the definition of signal-to-noise used for comments below.

2.2.3. Advantages of z-scrambling

(i) The angular positions are used because the angular selection function of the 2QZ is difficult to quantify by any other method, as stated above (a), in Sect. 1.

(ii) The use of z-scrambling (Osmer 1981) is adopted for obtaining the "random" redshift distributions, as in Roukema & Mamon (2001), in order to avoid redshift selection effects, as mentioned above in (c) of Sect. 1 (cf. Scott 1991).

The problems of incompleteness (b) are also minimised by this method of generating the random distributions.

Note that incompleteness is more likely to lead to noise than to spurious effects: if a "void" traced by quasars has several quasars missing, then it will be poorly traced, but will not be changed in diameter.

This method implies conservative results. Since some of the real, very large scale (e.g. $\sim 1\ h^{-1}\,$Gpc), but small amplitude correlations which may occur in the radial direction occur in both the real and the so-called random catalogues, these will cancel out along with the selection effect correlations that are (deliberately) cancelled, and be lost from the final signal. (These very large scale correlation cannot occur in the tangential direction in the 2QZ–10K, because of the angular selection function and division into six sub-samples by angle.)

So, this is an advantage in the sense that selection effects are cancelled; but can also be seen as a disadvantage in that the amplitude of real, non-zero values in the correlation function, in particular on large scales, may be underestimated. Since the phenomenon of interest here is the use of *local* feature(s) (first derivatives) in the correlation function as a standard ruler for obtaining geometrical constraints, the advantage largely outweighs the disadvantage: the method is conservative.

While absolute estimates of the correlation function (or power spectrum) clearly have cosmological relevance, the optimal methods for correcting for angular and redshift selection effects are likely to be considerably different from the method adopted here, and are not considered in this paper.

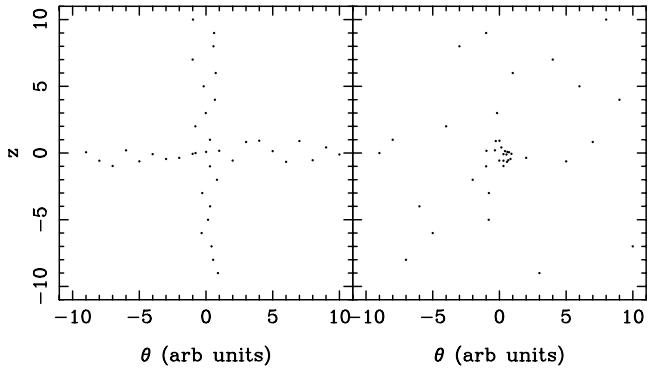

Fig. 1. Toy model showing why small scale correlations can be underestimated by z-scrambling when correlated structures exist on the scale of the survey volume and parallel to the θ and z directions (Sect. 2.2.4). The left-hand panel shows a toy model with filaments, parallel to these two directions, and each composed of 20 points. The right-hand panel shows a z-scramble of the distribution in the left-hand panel. The two "favoured" values of $\theta \approx 0$ and $z \approx 0$ in the original filaments (length units are arbitrary in the two directions) result in many z-scrambled pairs containing both these "favoured" values. Hence, many more *close* pairs exist in the z-scrambled distribution than in the original, correlated distribution. So, relative to the z-scrambled distribution, the original distribution is anti-correlated for pair separations up to the scale of the filament thickness, leading to underestimates of ξ on these small scales.

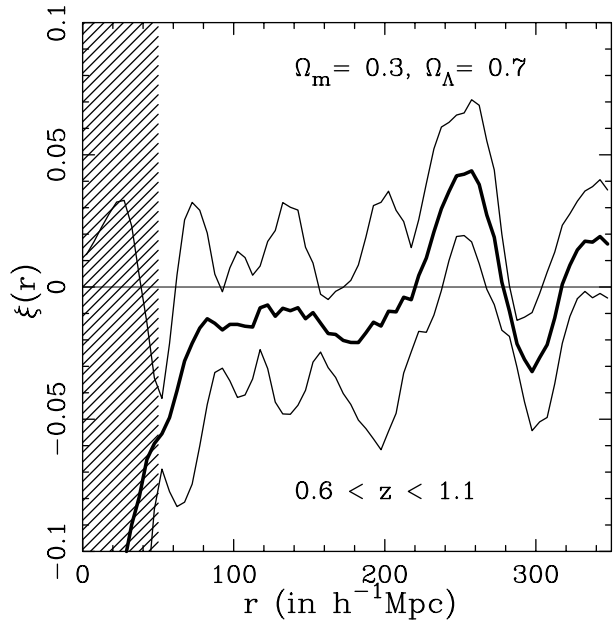

Fig. 2. The low-z ($0.6 < z < 1.1$) spatial two-point autocorrelation function $\xi(r)$, (Groth & Peebles 1977), for separations r in comoving units, for a flat universe with ($\Omega_{\rm m} = 0.3, \Omega_\Lambda = 0.7$). The $\sigma(r) = 15\,h^{-1}\,$Mpc Gaussian smoothed mean $\langle\xi\rangle$ and error bars corresponding to the standard error in the mean $\sigma_{\langle\xi\rangle}$ are shown by the thick and thin solid lines respectively. The small scale $r \lesssim 25$–$50\,h^{-1}\,$Mpc correlation is underestimated (hence the shading) due to the effect of z-scrambling in a survey of narrow beam width containing filaments (see Sect. 2.2.4 and Fig. 1 for details).

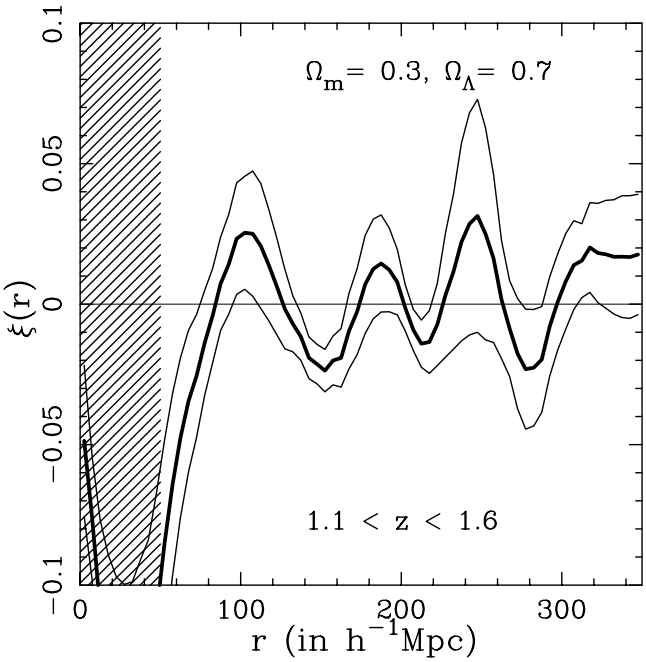

Fig. 3. The med-z ($1.1 < z < 1.6$) spatial two-point autocorrelation function $\xi(r)$, (Groth & Peebles 1977), for separations r in comoving units, for a flat universe with ($\Omega_m = 0.3, \Omega_\Lambda = 0.7$), as for Fig. 2.

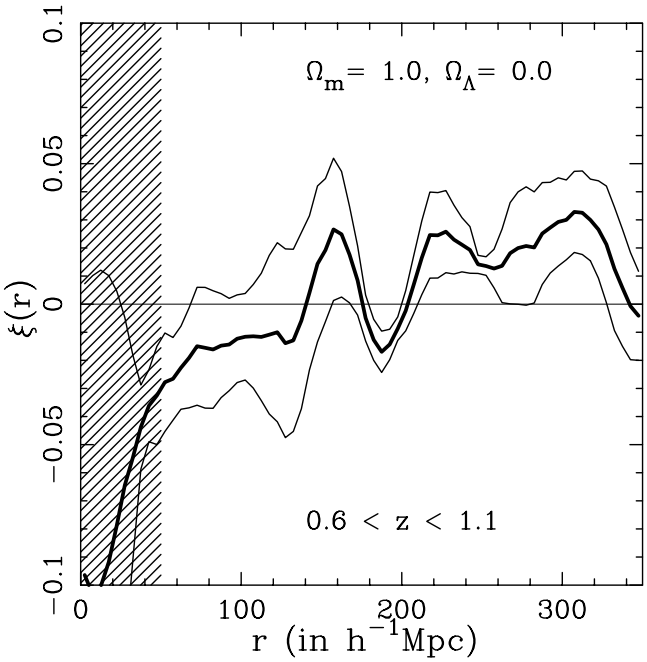

Fig. 5. The low-z ($0.6 < z < 1.1$) spatial two-point autocorrelation function $\xi(r)$, (Groth & Peebles 1977), for separations r in comoving units, for a flat universe with ($\Omega_m = 1.0, \Omega_\Lambda = 0.0$), as for Fig. 2.

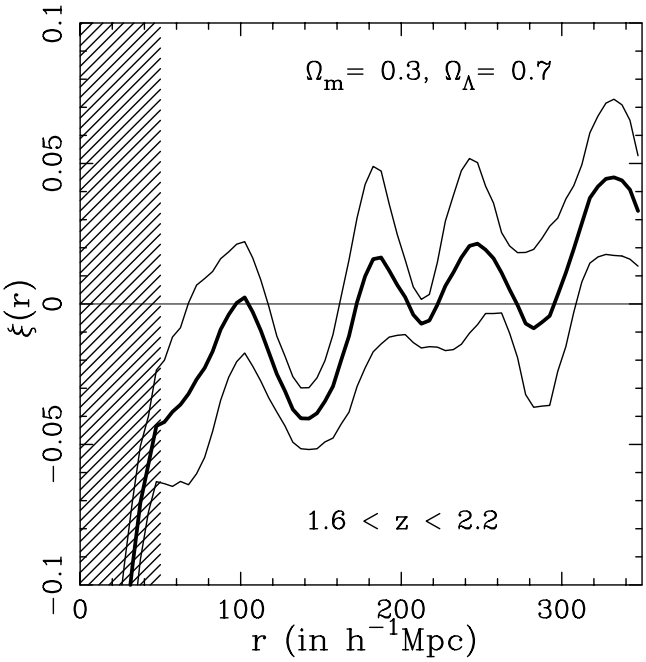

Fig. 4. The hi-z ($1.6 < z < 2.2$) spatial two-point autocorrelation function $\xi(r)$, (Groth & Peebles 1977), for separations r in comoving units, for a flat universe with ($\Omega_m = 0.3, \Omega_\Lambda = 0.7$), as for Fig. 2.

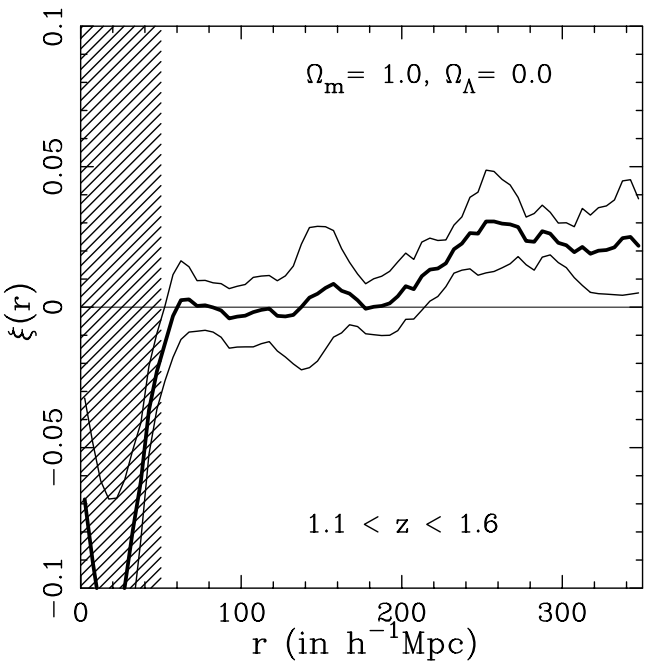

Fig. 6. The med-z ($1.1 < z < 1.6$) spatial two-point autocorrelation function $\xi(r)$, (Groth & Peebles 1977), for separations r in comoving units, for a flat universe with ($\Omega_m = 1.0, \Omega_\Lambda = 0.0$), as for Fig. 2.

2.2.4. Small r disadvantage of z-scrambling

The z-scrambling technique can have a disadvantage if

(i) either selection effect correlations or intrinsic correlations exist on a scale comparable to that of two of the dimensions of the survey volume, *and*

(ii) these correlations occur as filaments which are in some cases aligned with the tangential (θ) and radial (z) directions.

The effect is an overestimate of the numbers of close pairs in the random simulations, on the scale of the "thickness"

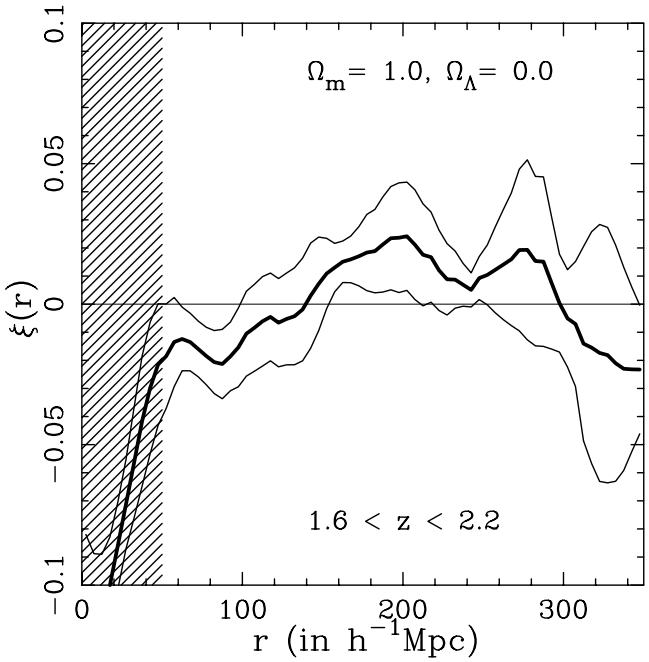

Fig. 7. The hi-z ($1.6 < z < 2.2$) spatial two-point auto-correlation function $\xi(r)$, (Groth & Peebles 1977), for separations r in comoving units, for a flat universe with ($\Omega_{\rm m} = 1.0, \Omega_\Lambda = 0.0$), as for Fig. 2.

of the "filaments", and, hence, an underestimate of $\xi(r)$ on scales r smaller than the "filament thickness".

This is illustrated in a toy model in Fig. 1, with a qualitative explanation in the caption.

An algebraic explanation of the effect can be made by writing the original distribution as points f_1^i in filament 1 and points f_2^i in filament 2, at approximately Cartesian coordinates (θ, z) for $i = 1, 10$:

$$f_1^i \approx (0, \pm i)$$
$$f_2^i \approx (\pm i, 0) \quad (5)$$

where "≈" indicates that the filaments are of about 1 length unit in thickness.

The z-scrambled distribution then contains many points

$$g^j \approx (0, 0) \quad (6)$$

which are strongly correlated [around the point $(0, 0)$] on a scale up to about 1 unit, even though the original distribution only contained about one point in this region.

This was not a serious problem for the Iovino et al. (1996) sample, since all the survey dimensions were well above $\sim$100–200 h^{-1} Mpc.

Here, however, the 2QZ–10K patches (see Fig. 1 of Croom et al. 2001) are about 2 degrees in size, corresponding to $\sim$50–100 h^{-1} Mpc in the $0.6 < z < 2.2$ redshift range, depending on the values of the local cosmological parameters. It is likely that at least some genuine filaments happen to lie in the radial and/or tangential directions, and some of the redshift selection effects (Scott 1991) are likely to create statistical excesses of quasars at certain favoured redshifts, i.e. creating what could be called "selection effect filaments" in the tangential direction.

What is the thickness of a filament, as traced by quasars? A minimum thickness is that corresponding to a few times the scale of the non-linear correlation length, $r_0 \sim 5\,h^{-1}$ Mpc, a maximum thickness is about 50% of typical void sizes, i.e. 50% of $\sim$50–100 h^{-1} Mpc, i.e. $r \lesssim 25$–$50\,h^{-1}$ Mpc.

This is the scale up to which an underestimate of $\xi(r)$ is possible. On larger scales, there should be a smooth transition to a slight overestimate of $\xi(r)$, due to pair conservation.

Since small scale correlations are subject to redshift evolution and the effects of non-linear growth of structure, they would require model-dependent interpretations if they were to be used for comoving standard ruler tests. So, the possible anti-correlation on small scales, due to z-scrambling in a survey with small dimensions, only affects the part of $\xi(r)$ which is most difficult to use, and should not be a problem for the present paper.

3. Results

3.1. Correlation functions

Figures 2–7 show the correlation functions $\xi(r)$ for the low-z, med-z and hi-z redshift intervals of the 2QZ–10K, for the local metric parameter values ($\Omega_{\rm m} = 0.3, \Omega_\Lambda = 0.7$) favoured from other observations, and for the now disfavoured Einstein-de Sitter metric ($\Omega_{\rm m} = 1.0, \Omega_\Lambda = 0.0$).

Keeping in mind that the method of calculation of $\xi(r)$ adopted here, which uses z-scrambling, is conservative and is likely to imply cancellation of some real correlations, i.e. to underestimate the amplitudes of the correlations, and that either real or selection effect structures in the data are likely to cause an anti-correlation at small-scales, as indicated by the shading at $r \lesssim 50\,h^{-1}$ Mpc in Figs. 2–7, the following are clear from the figures:

(i) A local maximum at a fixed comoving scale, $r \approx 240\,h^{-1}$ Mpc, is clearly present in all three redshift ranges for ($\Omega_{\rm m} = 0.3, \Omega_\Lambda = 0.7$), at signal-to-noise ratios (defined in Eq. (4)) of $(S/N) = 2.4$, $(S/N) = 1.1$ and $(S/N) = 1.6$ at low-z, med-z and hi-z respectively.

(ii) A local maximum at a fixed comoving scale, $r \approx 180\,h^{-1}$ Mpc, is present in the two higher redshift ranges for ($\Omega_{\rm m} = 0.3, \Omega_\Lambda = 0.7$), at a signal-to-noise ratio of $(S/N) = 1.4$ at med-z and $(S/N) = 1.7$ at hi-z, but absent in the low-z data.

(iii) A local maximum at a fixed comoving scale, $r \approx 90\,h^{-1}$ Mpc, is present in the two higher redshift ranges for ($\Omega_{\rm m} = 0.3, \Omega_\Lambda = 0.7$), but absent in the low-z data.

(iv) The anti-correlation at $r \lesssim 50\,h^{-1}$ Mpc expected, due to "aligned filaments", the survey geometry and z-scrambling, is present at these scales, for both choices of local cosmological parameters. This implies

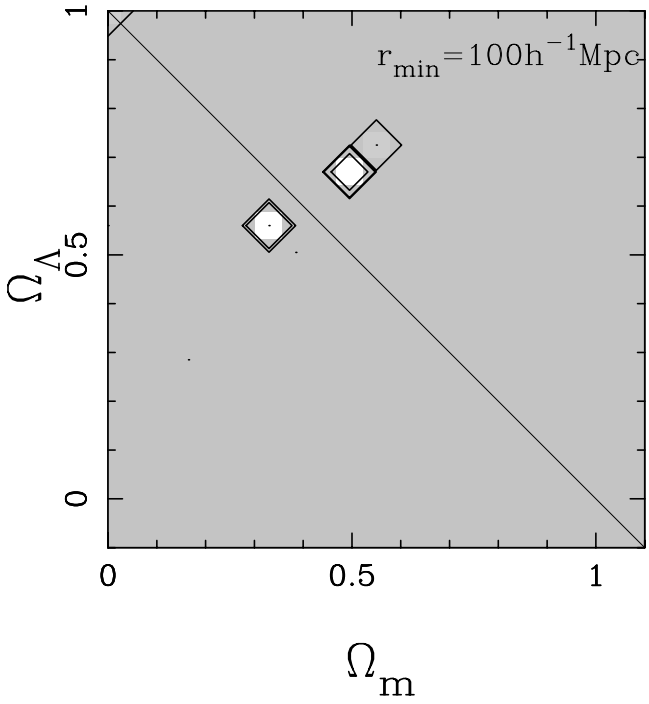

Fig. 8. Confidence intervals for rejecting the hypothesis that the first local maximum in the spatial correlation function at $r > 100\,h^{-1}$ Mpc occurs at the same comoving position in the low-z, med-z and hi-z redshift intervals of the 2QZ–10K, for various hypotheses on the values of $(\Omega_{\rm m}, \Omega_\Lambda)$. The uncertainty in the estimate of the position of a local maximum is $\Delta L_{\rm LSS} = 5\,h^{-1}$ Mpc. Rejection levels of 68% $> 1-P$, 95% $> 1-P$, 99.7% $> 1-P$ and $1-P > 99.7$ are indicated in this figure and in Figs. 9, 10, with gray shadings from white to gray as a visual aid. In this figure, the two white squares indicate $(\Omega_{\rm m}, \Omega_\Lambda)$ values satisfying 68% $> 1-P$, and nearly all of the figure lies in the $1-P > 99.7$ domain. Due to stronger signals in Figs. 9, 10, the contours in these figures are better labelled. A thin line indicating a flat universe ($\Omega_{\rm m} + \Omega_\Lambda = 1$) is indicated in this and the following figures.

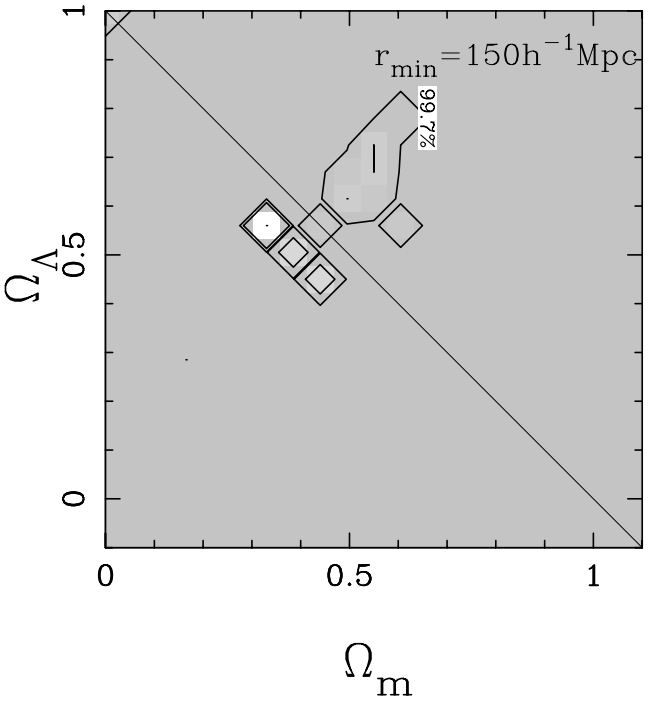

Fig. 9. As for Fig. 8, confidence intervals for rejecting the hypothesis that the first local maximum in the spatial correlation function at $r > 150\,h^{-1}$ Mpc in all three redshift intervals.

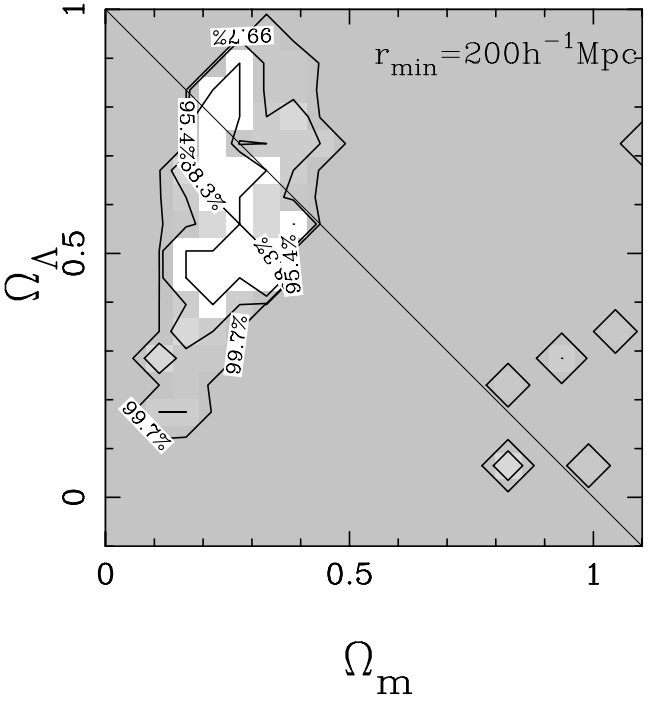

Fig. 10. As for Fig. 8, confidence intervals for rejecting the hypothesis that the first local maximum in the spatial correlation function at $r > 200\,h^{-1}$ Mpc in all three redshift intervals.

a risk of systematic error if the $r \approx 90\,h^{-1}$ Mpc maximum were to be used for the consistency of comoving scale test, since it could be strongly affected by this effect. So, the conservative approach of using $r_{\rm min}$ values of $100, 150$ and $200\,h^{-1}$ Mpc will be retained here.

(v) The low-z correlation function for $(\Omega_{\rm m} = 1.0, \Omega_\Lambda = 0.0)$, Fig. 5, clearly shows local maxima resembling those in the low-z $(\Omega_{\rm m} = 0.3, \Omega_\Lambda = 0.7)$ correlation function, but displaced to smaller separations. In contrast, the med-z and hi-z correlation functions for $(\Omega_{\rm m} = 1.0, \Omega_\Lambda = 0.0)$ only show broad, more or less flat features.

(vi) The best sign of a feature at a consistent comoving scale for $(\Omega_{\rm m} = 1.0, \Omega_\Lambda = 0.0)$ is the $(S/N) \approx 2$ maximum at $r \approx 160\,h^{-1}$ Mpc in the low-z correlation function, and the $(S/N) \approx 0.5$ maximum at $r \approx 150\,h^{-1}$ Mpc in the med-z correlation function. Since low (S/N) has not been used as a criterion for excluding maxima, these two features could have, in principle, provided an argument in favour of this choice of metric parameters, according to the method defined above, if the feature were also present in the hi-z sample. However, it does not appear to be present in the hi-z sample, and as is seen below

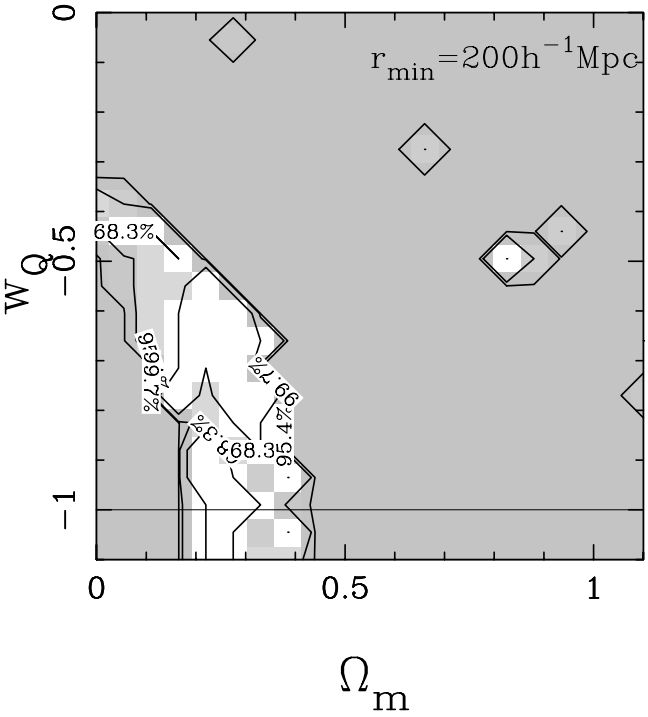

Fig. 11. As for Fig. 8, confidence intervals for rejecting the hypothesis of a local correlation function maximum at $r > 200\,h^{-1}$ Mpc present in all three 2QZ–10K redshift intervals, for a flat, effective quintessence model, for various hypotheses on the values of $(\Omega_{\rm m}, w_{\rm Q})$. A thin line where $w_{\rm Q} \equiv 1$, i.e. equivalent to a cosmological constant model, is indicated in the figure.

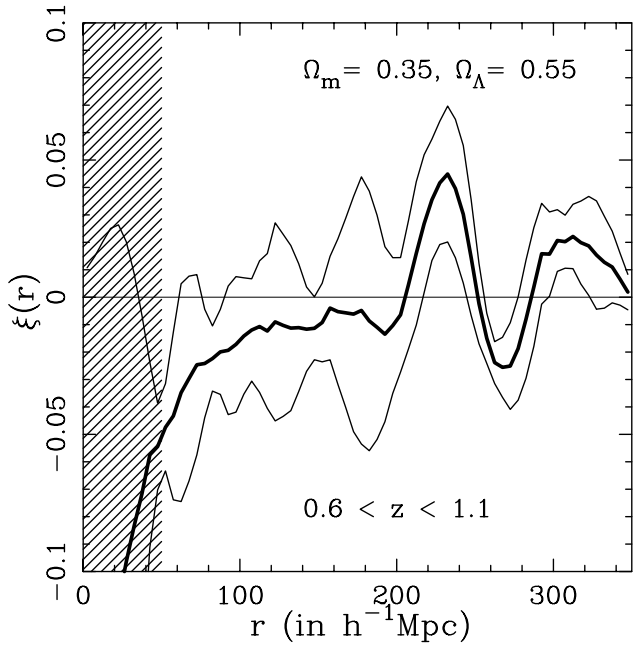

Fig. 12. The low-z ($0.6 < z < 1.1$) spatial two-point autocorrelation function $\xi(r)$, for an hyperbolic universe with $(\Omega_{\rm m} = 0.35, \Omega_\Lambda = 0.55)$, as for Fig. 2.

quantitatively, is rejected as a maximum present in all three redshift ranges.

3.2. Comoving consistency of the position of a local maximum at all redshifts

Figures 8–10 show the confidence levels for rejecting the hypothesis that a local maximum is present in all three redshift intervals, for $r_{\rm min} = 100\,h^{-1}$ Mpc, $r_{\rm min} = 150\,h^{-1}$ Mpc and $r_{\rm min} = 200\,h^{-1}$ Mpc, i.e. without preselecting a particular scale.

For $r_{\rm min} = 100\,h^{-1}$ Mpc and $r_{\rm min} = 150\,h^{-1}$ Mpc, only one or two solutions exist. The solution in common to both, and also consistent with the test for $r_{\rm min} = 200\,h^{-1}$ Mpc, is that with $(\Omega_{\rm m} \approx 0.35, \Omega_\Lambda \approx 0.55)$. The $r_{\rm min} = 200\,h^{-1}$ Mpc test provides a much larger range of consistent solutions, consistent with the flat, $(\Omega_{\rm m} = 0.3, \Omega_\Lambda = 0.7)$ metric, but favouring a hyperbolic metric (commonly called an "open" metric, either "open open" or "closed open"; see Luminet & Roukema 1999 or Roukema 2000 to see why an "open" universe may be either open or closed).

The reason for the different sizes of the 68% contours in these plots are clear from the correlation functions (Figs. 2–7). The maximum at $r \approx 240\,h^{-1}$ Mpc for $(\Omega_{\rm m} = 0.3, \Omega_\Lambda = 0.7)$ is clearly present in all three redshift ranges (Figs. 2–4), but in the low redshift range for these metric parameters (Fig. 2), only slight, noisy ripples, much smaller than the error bars, are present above $100\,h^{-1}$ Mpc and $150\,h^{-1}$ Mpc for matching the $r \approx 180\,h^{-1}$ Mpc maximum in the med-z and hi-z samples.

Figure 12 shows why a consistent solution is found at $(\Omega_{\rm m} \approx 0.35, \Omega_\Lambda \approx 0.55)$: a local maximum in the range $160 < r < 180\,h^{-1}$ Mpc is present, though it is not significant given the error bars. Both the $r_{\rm min} = 100$ and $r_{\rm min} = 150$ tests consider this peak to be consistent with the $r \approx 180\,h^{-1}$ Mpc in the med-z and hi-z redshift samples. It is clear that this is not a significant solution.

It is also clear that no local maximum is common to all three redshift ranges for the Einstein-de Sitter metric $(\Omega_{\rm m} = 1.0, \Omega_\Lambda = 0.0)$, nor for a low matter density model with zero cosmological constant $(\Omega_{\rm m} = 0.3, \Omega_\Lambda = 0.0)$.

3.3. What are the implied constraints on the metric parameters?

Given that the $r \sim 180\,h^{-1}$ Mpc maximum providing the solution in Figs. 8 and 9 has a low signal-to-noise ratio, and that the $r \approx 240\,h^{-1}$ Mpc clearly has the strongest signal-to-noise ratio in all redshift ranges, the most robust constraint on the metric parameters is that of Fig. 10.

This result is

$$\Omega_{\rm m} = 0.25 \pm 0.10 \ \ (68\%\ \text{confidence})$$

$$\Omega_{\rm m} = 0.25 \pm 0.15 \ \ (95\%\ \text{confidence})$$

$$\Omega_\Lambda = 0.65 \pm 0.25 \ \ (68\%\ \text{confidence})$$

$$\Omega_\Lambda = 0.60 \pm 0.35 \ \ (95\%\ \text{confidence}). \qquad (7)$$

The length scale of the local maximum is also constrained. The 68% and 95% confidence intervals imply nearly identical estimates and uncertainties in the length scale of the

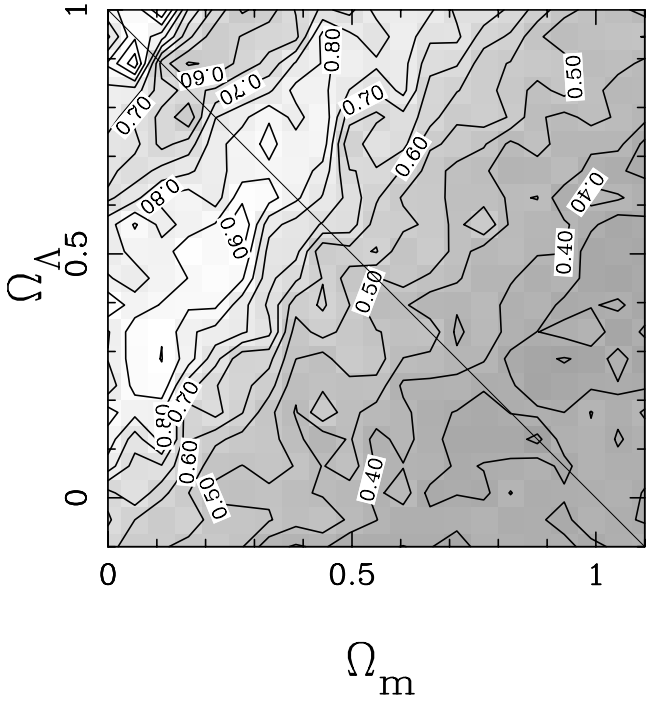

Fig. 13. Values of the difference statistic D (Eq. (16)), representing the average absolute slope of $\xi(r)$ in the interval $200\,h^{-1}\,\mathrm{Mpc} \leq r \leq 300\,h^{-1}\,\mathrm{Mpc}$ over all three redshift intervals, which would depend monotonically on Ω_m and Ω_Λ if fluctuations in this interval were due only to noise and not to a genuine cosmological signal. The maximum value of D is $D = 1$. Contours from $D = 0.4$ to $D = 0.9$, in intervals of $\Delta D = 0.05$ are indicated. Shading is darker for lower values of D. It is clear that D does not increase monotonically from $(\Omega_\mathrm{m} = 1.1, \Omega_\Lambda = -0.1)$ to $(\Omega_\mathrm{m} = 0.0, \Omega_\Lambda = 1.0)$. The excess values of D, i.e. the excess average absolute differences, with respect to the underlying trend, occur in a region peaked at $(\Omega_\mathrm{m} \approx 0.25, \Omega_\Lambda \approx 0.55)$.

local maximum, which can be labelled $2L_\mathrm{LSS}$ because of its similarity to twice the length scale claimed in many other studies at low redshift. The scale is estimated by taking the mean and standard deviation of the values r^i_max of the local maximum for the three redshift intervals, either with or without weighting by the rejection probability, within either the $1 - P = 68\%$ or the $1 - P = 95\%$ confidence contour.

This formally yields

$$
\begin{aligned}
2L_\mathrm{LSS} &= 242.9 \pm 16.1\,h^{-1}\,\mathrm{Mpc} \ \ (68\%\ \text{confidence})\\
2L_\mathrm{LSS} &= 243.0 \pm 16.6\,h^{-1}\,\mathrm{Mpc} \ \ (95\%\ \text{confidence})\\
2L_\mathrm{LSS} &= 244.4 \pm 16.5\,h^{-1}\,\mathrm{Mpc}\\
&\quad (68\%\ \text{confidence, weighted})\\
2L_\mathrm{LSS} &= 244.3 \pm 16.7\,h^{-1}\,\mathrm{Mpc}\\
&\quad (95\%\ \text{confidence, weighted}) \qquad (8)
\end{aligned}
$$

which can be summarised as

$$L_\mathrm{LSS} = 122 \pm 9\,h^{-1}\,\mathrm{Mpc} \ \ (95\%). \qquad (9)$$

A similar hypothesis test to the above for $r_\mathrm{min} = 200\,h^{-1}\,\mathrm{Mpc}$, i.e. using the $r \approx 240\,h^{-1}\,\mathrm{Mpc}$ local maximum, but for a flat metric in an effective quintessence model has also been performed (Fig. 11). This yields

$$
\begin{aligned}
\Omega_\mathrm{m} &= 0.25 \pm 0.10 \ \ (68\%\ \text{confidence})\\
\Omega_\mathrm{m} &= 0.2 \pm 0.2 \ \ (95\%\ \text{confidence})\\
w_\mathrm{Q} &< -0.5 \ \ (68\%\ \text{confidence}) \qquad (10)\\
w_\mathrm{Q} &< -0.35 \ \ (95\%\ \text{confidence}). \qquad (11)
\end{aligned}
$$

The introduction of external constraints would strengthen these results, e.g. $\Omega_\mathrm{m} \geq 0.2$ would imply $w_\mathrm{Q} < -0.5$ (95% confidence), but for this study it is preferred to deduce constraints independently of other observational analyses.

4. Discussion

Is the local maximum found at $2L_\mathrm{LSS} = 244 \pm 17\,h^{-1}\,\mathrm{Mpc}$ in all three redshift ranges for $(\Omega_\mathrm{m} \approx 0.25, \Omega_\Lambda \approx 0.65)$ a real, cosmological signal or could it just be noise which happens to give the signal expected? Answers to this question can be divided according to whether or not and which external information is accepted as a valid prior assumption.

There are strong observational justifications for expecting that $\Omega_\mathrm{m} \approx 0.3$, $\Omega_\Lambda \approx 0.7$, and there are also numerous observational analyses in favour of fine features in the power spectrum or correlation of density perturbations as traced by extragalactic objects, in particular, in favour of a local maximum at $L_\mathrm{LSS} \approx 130 \pm 10\,h^{-1}\,\mathrm{Mpc}$. The former are close to being widely accepted by many independent groups, but the latter remain controversial.

So, the reality of the signal can be discussed in the context of

(i) no assumption regarding $\Omega_\mathrm{m}, \Omega_\Lambda, L_\mathrm{LSS}$; or
(ii) the assumption that $\Omega_\mathrm{m} \approx 0.3, \Omega_\Lambda \approx 0.7$, but no assumption regarding L_LSS; or
(iii) the assumption that $L_\mathrm{LSS} \approx 130 \pm 10\,h^{-1}\,\mathrm{Mpc}$, but no assumptions regarding $\Omega_\mathrm{m}, \Omega_\Lambda$; or
(iv) the assumptions that $\Omega_\mathrm{m} = 0.25, \Omega_\Lambda = 0.65$ and $2L_\mathrm{LSS} = 244 \pm 17\,h^{-1}\,\mathrm{Mpc}$.

4.1. (i) No assumption regarding $\Omega_m, \Omega_\Lambda, L_{LSS}$

Let us make no assumption regarding $\Omega_\mathrm{m}, \Omega_\Lambda$ and L_LSS.

Consider the dependence of an arbitrary property of $\xi(r)$, represented by some statistic of $\xi(r)$, as a function of Ω_m and Ω_Λ.

The value of $\xi(r)$ in any bin depends on the numbers of pairs falling in the bin, i.e. on the numbers of "data-data" (DD) pairs, "data-random" (DR) pairs, and "random-random" (RR) pairs.

For a fixed distribution in redshift and angular position, as Ω_m decreases and/or as Ω_Λ increases, the proper distance separation between any given pair of quasars increases. So, as Ω_m decreases and/or as Ω_Λ increases,

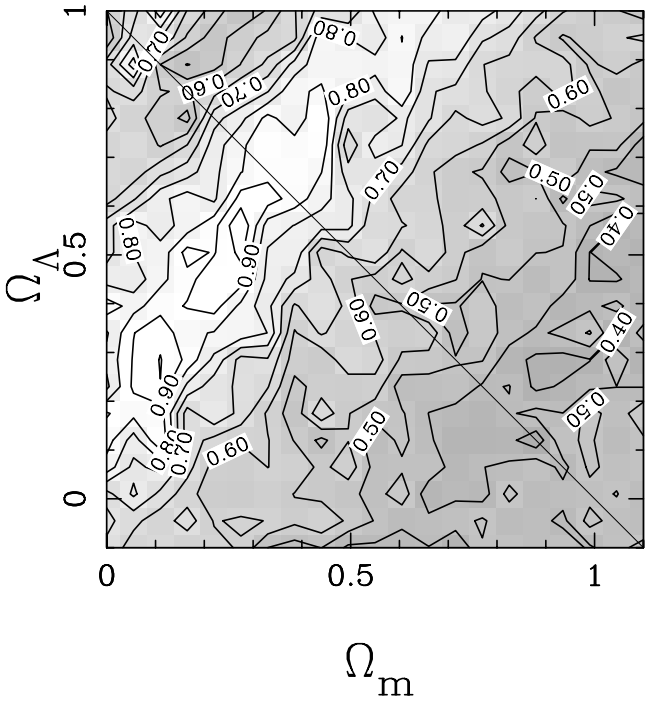

Fig. 14. Values of the Poisson-corrected difference statistic D' (Eq. (17)), as for Fig. 13, but where D is approximately corrected for the monotonic variation as a function of expected Poisson noise, yielding D'. It is clear that excess values of D' occur near ($\Omega_\mathrm{m} \approx 0.25, \Omega_\Lambda \approx 0.55$) and pass through a linear degeneracy from this point to ($\Omega_\mathrm{m} \approx 0.1, \Omega_\Lambda \approx 0.3$). This confirms that a non-Poisson signal is present in $\xi(r)$ for a pair $(\Omega_\mathrm{m}, \Omega_\Lambda)$ lying somewhere in this degeneracy region.

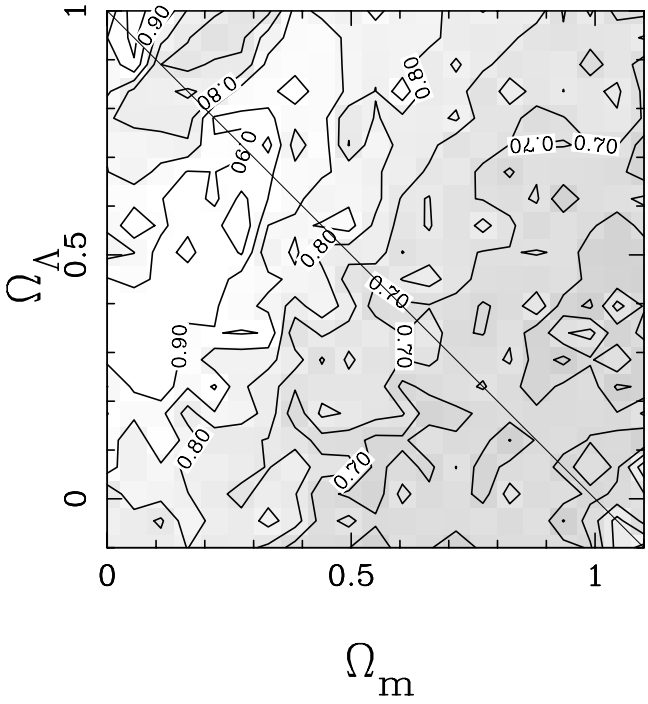

Fig. 15. Values of the Poisson-corrected difference statistic D', as for Fig. 14, but for the interval $100\,h^{-1}\,\mathrm{Mpc} \leq r \leq 350\,h^{-1}\,\mathrm{Mpc}$. The excess values of D' seen in Fig. 14 near ($\Omega_\mathrm{m} \approx 0.25, \Omega_\Lambda \approx 0.55$) remain present. Imperfect correction for the Poisson error also yields a background which is not quite flat, so that high D' values also appear near $\Omega_\mathrm{m} \approx 0.05, \Omega_\Lambda \gtrsim 0.95$, but are due to Poisson error and not an excess relative to Poisson error.

the full distribution of pair separations is stretched over a larger interval of proper separations, and the Poisson error per bin increases. This stretching is mostly in the radial direction, since the radial sizes of the densely observed regions of the 2QZ–10K are about an order of magnitude greater than their tangential sizes.

This can be shown algebraically as follows. Ignoring the angular separations, since these are small, the full pair distribution is spread over the interval which is approximately

$$0 \leq r \leq d(\Omega_\mathrm{m}, \Omega_\Lambda, z_2) - d(\Omega_\mathrm{m}, \Omega_\Lambda, z_1) \qquad (12)$$

where $d(\Omega_\mathrm{m}, \Omega_\Lambda, z_i)$ are the proper distances from the observer to the redshift limits z_i. The number of pairs m in any given separation bin is

$$m \propto \frac{1}{d(\Omega_\mathrm{m}, \Omega_\Lambda, z_2) - d(\Omega_\mathrm{m}, \Omega_\Lambda, z_1)}. \qquad (13)$$

So, the fractional Poisson error per bin is

$$\frac{\Delta m}{m} \propto \sqrt{d(\Omega_\mathrm{m}, \Omega_\Lambda, z_2) - d(\Omega_\mathrm{m}, \Omega_\Lambda, z_1)}. \qquad (14)$$

Thus, the Poisson error per bin increases when Ω_m decreases and/or Ω_Λ increases (see Eqs. (1), (2)).

If $\xi(r)$ has no fine scale features, i.e. only noise fluctuations, then the increase in Poisson error should be the only systematic effect of changing Ω_m and/or Ω_Λ, and it should be a *monotonic* effect, in the sense that the highest amount of noise should occur for the lowest Ω_m and the highest Ω_Λ calculations.

The favoured values of Ω_m and Ω_Λ found above (Eq. (7)) are *not* the lowest and highest (respectively) of the domain investigated. This provides one argument against the local maximum at $2L_\mathrm{LSS} = 244 \pm 17\,h^{-1}\,\mathrm{Mpc}$ being a noise fluctuation.

An independent argument is to define a difference statistic

$$D_0(\Omega_\mathrm{m}, \Omega_\Lambda) \equiv \sum_{r_1}^{r_2} |\xi(r + \Delta r, \Omega_\mathrm{m}, \Omega_\Lambda) - \xi(r, \Omega_\mathrm{m}, \Omega_\Lambda)| \qquad (15)$$

and its normalised value

$$D(\Omega_\mathrm{m}, \Omega_\Lambda) \equiv \frac{D_0(\Omega_\mathrm{m}, \Omega_\Lambda)}{\max_{\Omega_\mathrm{m}, \Omega_\Lambda}\{D_0(\Omega_\mathrm{m}, \Omega_\Lambda)\}}, \qquad (16)$$

over a range of pair separations $r_1 \leq r \leq r_2$. The limits r_1, r_2 can be chosen in order to answer the question raised above regarding the $2L_\mathrm{LSS}$ local maximum, i.e. $r_1 = 200\,h^{-1}\,\mathrm{Mpc}$, $r_2 = 300\,h^{-1}\,\mathrm{Mpc}$, or can be chosen to further remove prior knowledge of $2L_\mathrm{LSS}$ while remaining in a domain where noise signals are least likely to occur, i.e. $r_1 = 100\,h^{-1}\,\mathrm{Mpc}$, $r_2 = 350\,h^{-1}\,\mathrm{Mpc}$.

This statistic does *not* contain any information on whether or not a local maximum is present in this range. It can be said to represent the average absolute value of the slope of $\xi(r)$, or more informally, how much $\xi(r)$ fluctuates.

If only noise is present, then D should vary monotonically as a function of Ω_m and Ω_Λ, since the slopes of $\xi(r)$ would only be noise-generated.

On the other hand, if a cosmological fluctuation in $\xi(r)$ is present in the data, then whether or not it's a local maximum, a local minimum or just the rising or falling slope of one or the other, the values of D near the correct values of $(\Omega_\mathrm{m}, \Omega_\Lambda)$ should be higher than for surrounding values of $(\Omega_\mathrm{m}, \Omega_\Lambda)$.

An approximate correction for the monotonic variation in D, due to the decreased numbers of pairs per bin and resulting increased (fractional) Poisson errors for lower Ω_m and higher Ω_Λ values, can be made by using dependence of the maximum proper distance, $d(\Omega_\mathrm{m}, \Omega_\Lambda, z)$, across the full redshift range, and replacing D by

$$D'(\Omega_\mathrm{m}, \Omega_\Lambda) \equiv D(\Omega_\mathrm{m}, \Omega_\Lambda) \left[\frac{d(\Omega_\mathrm{m}, \Omega_\Lambda, 2.2) - d(\Omega_\mathrm{m}, \Omega_\Lambda, 0.6)}{d(0.0, 1.1, 2.2) - d(0.0, 1.1, 0.6)} \right]^{-1/2} . \quad (17)$$

Figure 13 shows the dependence of D on Ω_m and Ω_Λ.

Instead of D increasing smoothly and monotonically from $(\Omega_\mathrm{m} = 1.1, \Omega_\Lambda = -0.1)$ to $(\Omega_\mathrm{m} = 0.0, \Omega_\Lambda = 1.0)$, as would be the case if fluctuations were only caused by noise, it is clear that D does *not* vary monotonically with Ω_m and Ω_Λ.

Moreover, the exceptional region is clearly that of the excess values of D surrounding $(\Omega_\mathrm{m} \approx 0.25, \Omega_\Lambda \approx 0.55)$. It is not possible that the region $\Omega_\mathrm{m} \approx 0.15, \Omega_\Lambda \approx 0.8$ is a dip relative to the noise values of D, since any additional component to D not caused by noise must cause a positive contribution (absolute values are always non-negative).

The approximate correction for the monotonic dependence on Poisson noise (Eq. (17)) shows this excess signal even more clearly, in D', shown in Figs. 14 and 15. Although the Poisson noise dependence is not completely removed, since the correction applied is only approximate, it is clear that D' has excessively large values in the linear region from $(\Omega_\mathrm{m} \approx 0.25, \Omega_\Lambda \approx 0.55)$ to $(\Omega_\mathrm{m} \approx 0.1, \Omega_\Lambda \approx 0.3)$, and that this is the case whether or not a relatively small region around the $2L_\mathrm{LSS} = 244 \pm 17\,h^{-1}\,\mathrm{Mpc}$ maximum, i.e. $200\,h^{-1}\,\mathrm{Mpc} \leq r \leq 300\,h^{-1}\,\mathrm{Mpc}$ (Fig. 14), or a relatively large region around the maximum, i.e. $100\,h^{-1}\,\mathrm{Mpc} \leq r \leq 350\,h^{-1}\,\mathrm{Mpc}$ (Fig. 15), is used.

It is difficult to explain these excess values of D' unless *there is a cosmological signal for some* $(\Omega_\mathrm{m}, \Omega_\Lambda)$ *pair in the degeneracy region from* $(\Omega_\mathrm{m} \approx 0.25, \Omega_\Lambda \approx 0.55)$ *to* $(\Omega_\mathrm{m} \approx 0.1, \Omega_\Lambda \approx 0.3)$.

Suppose a metric value pair outside of this region, e.g. $(\Omega_\mathrm{m} \approx 1.0, \Omega_\Lambda \approx 0.0)$, is valid. Then, either

(a) there is a fluctuation of cosmological origin in $\xi(r)$ of the 2QZ–10K, or

(b) there is not, i.e. there is only noise.

Consider each case.

(a) If $(\Omega_\mathrm{m} \approx 1.0, \Omega_\Lambda \approx 0.0)$ and there is a cosmological fluctuation in $\xi(r)$, then there must be an excess value of D and D' near $(\Omega_\mathrm{m} \approx 1.0, \Omega_\Lambda \approx 0.0)$, since for any *wrong* value of $(\Omega_\mathrm{m}, \Omega_\Lambda)$, the "correlated pairs" which would have been placed in a single separation bin, say, the ith separation bin, $r_1 + (i-1)\Delta r < r < r_1 + i\Delta r$ [for $(\Omega_\mathrm{m} \approx 1.0, \Omega_\Lambda \approx 0.0)$], are diluted over several bins $\{r_1 + (i'-1)\Delta r < r < r_1 + i'\Delta r\}_{i'=i,i-1,i-2,\ldots,i+1,i+2,\ldots}$ and the value of D and D' is decreased. However, there is *not* an excess in D and D' at $(\Omega_\mathrm{m} \approx 1.0, \Omega_\Lambda \approx 0.0)$. So, case (a) is wrong.

(b) If $(\Omega_\mathrm{m} \approx 1.0, \Omega_\Lambda \approx 0.0)$ and and there is *no* cosmological fluctuation in $\xi(r)$, then the fluctuations in $\xi(r)$ are Poisson noise fluctuations. This noise must increase monotonically as Ω_m decreases and/or as Ω_Λ increases [Eq. (14)]. Hence, there must *not* be an excess of D and D' near $(\Omega_\mathrm{m} \approx 0.25, \Omega_\Lambda \approx 0.55)$, since this is far from the limit $(\Omega_\mathrm{m} = 0.0, \Omega_\Lambda = 1.0)$. However, there *is* an excess of D and D' near $(\Omega_\mathrm{m} \approx 0.25, \Omega_\Lambda \approx 0.55)$. So, case (b) is wrong.

Since both (a) and (b) are wrong, $(\Omega_\mathrm{m} \approx 1.0, \Omega_\Lambda \approx 0.0)$ is invalid independently of whether or not the existence of a fluctuation of cosmological origin is assumed.

The same argument holds for other pairs $(\Omega_\mathrm{m}, \Omega_\Lambda)$ outside of the degeneracy region from $(\Omega_\mathrm{m} \approx 0.25, \Omega_\Lambda \approx 0.55)$ to $(\Omega_\mathrm{m} \approx 0.1, \Omega_\Lambda \approx 0.3)$.

The only reasonable interpretation of Figs. 13–15 is that $(\Omega_\mathrm{m}, \Omega_\Lambda)$ lies in the degeneracy region from $(\Omega_\mathrm{m} \approx 0.25, \Omega_\Lambda \approx 0.55)$ to $(\Omega_\mathrm{m} \approx 0.1, \Omega_\Lambda \approx 0.3)$ and that $\xi(r)$ has at least some fluctuating component which is a comoving, cosmological signal and not Poisson noise.

4.2. (ii) The assumption that $\Omega_m \approx 0.3, \Omega_\Lambda \approx 0.7$, but no assumption regarding L_{LSS}

Given the prior estimate that $\Omega_\mathrm{m} \approx 0.3, \Omega_\Lambda \approx 0.7$, Figs. 2–4 show that a local maximum of signal-to-noise ratio (Eq. (4)) of $S/N \approx 3$, 1 and 1 exists near $2L_\mathrm{LSS} = 244 \pm 17\,h^{-1}\,\mathrm{Mpc}$ in the low, medium and high redshift ranges respectively.

Why should a local maximum due to noise occur at the same position in all three redshift ranges, to within the precision of one bin ($\Delta r = 5\,h^{-1}\,\mathrm{Mpc}$), if it were not physical?

The interval between successive maxima is at least $\approx 60\,h^{-1}\,\mathrm{Mpc}$. In the low redshift bin the interval is higher, since the larger error bars lead to insignificant maxima at lower length scales, but let us be conservative and adopt $60\,h^{-1}\,\mathrm{Mpc}$ as the scale along which a random maximum could occur. If it is assumed that local maxima occur about once within this interval but with random phase, then the chance of agreement between two redshift ranges to within $\pm 5\,h^{-1}\,\mathrm{Mpc}$ is then $P = 10/60$, and between all

three is $P = (10/60)^2 \approx 0.03$, i.e. the hypothesis of uniform random phases for these local maxima is rejected at the 97% confidence level.

The assumption that $\Omega_{\rm m} \approx 0.3, \Omega_\Lambda \approx 0.7$ also suggests that the local maxima which appear at $r \approx 100\,h^{-1}\,$Mpc and $r \approx 180\,h^{-1}\,$Mpc in the med-z and hi-z samples could be real.

The former is likely to be affected by the existence of correlated structures in a survey geometry of narrow dimensions and the use of z-scrambling (Sect. 2.2.4), so is unlikely to be cosmological in origin. The latter should be considered a better candidate for a real local maximum. However, given the lack of its detection in the low-z sample, it is more prudent to consider the 2QZ–10K data to be insufficient to establish its existence.

4.3. (iii) The assumption that $L_{LSS} \approx 130 \pm 10\ h^{-1}$ Mpc, but no assumptions regarding Ω_m, Ω_Λ

If the existence of a local maximum near $L_{\rm LSS} \approx 130 \pm 10\,h^{-1}\,$Mpc is assumed, then in the analysis discussed in Sect. 3.2 and shown in Figs. 8 and 12, a search for a consistent local maximum in the $(\Omega_{\rm m}, \Omega_\Lambda)$ plane for $r_{\rm min} = 100\,h^{-1}\,$Mpc should have led to a significant solution. However, only a weak solution exists, and Fig. 12 shows that this is for a local maximum at $160 < r < 180\,h^{-1}\,$Mpc rather than at $130 \pm 10\,h^{-1}\,$Mpc, with a negligible signal-to-noise ratio.

At first sight, this is, therefore, the most puzzling result of this analysis. If there are genuine fine features significantly detected in $\xi(r)$ of the 2QZ–10K, why should the most commonly claimed feature at low redshift be absent?

Two likely answers include:

(i) the sparsity of the sample, and/or
(ii) coincidence of genuine correlations with redshift and or angular selection effects

which are both capable of removing underlying matter density correlations from the sample. No amount of correction can (validly) re-introduce correlations which are absent from a catalogue due to one or both of these reasons.

Another possibility is:

(iii) that by use of z-scrambling and observational angular positions to mimic selection effects as closely as possible, the cosmological correlations have also been mimicked in the random catalogues and, hence, been cancelled out of $\xi(r)$.

Note that these effects are related to the use of a conservative technique: careful correction for selection effects risks cancelling some real, cosmological correlations, but implies that any detected signal is very unlikely to be a selection effect.

If one or several of the explanations (i)–(iii) are correct, then it should still be expected that if a local maximum is detected at a scale where sparsity or selection effects are less serious, it is detected at a harmonic of the assumed scale.

This is indeed the case. Without prior constraints on $(\Omega_{\rm m}, \Omega_\Lambda)$, a local maximum at the scale $2L_{\rm LSS} = 244 \pm 17\,h^{-1}\,$Mpc was detected.

This supports the claim that a local maximum in $\xi(r)$ or the power spectrum exists at $L_{\rm LSS} \approx 130 \pm 10\,h^{-1}\,$Mpc, and possibly provides a more accurate estimate ($L_{\rm LSS} = 122 \pm 9\,h^{-1}\,$Mpc) than the low redshift estimates, since the effects of peculiar velocities are much smaller than for the low redshift samples.

Earlier arguments related to (i) include the suggestion by de Lapparent et al. (1991) that the existence of a scale of $L_{\rm LSS} \sim 120\,h^{-1}\,$Mpc, traced by positive density fluctuations, is implied by the observed existence of large scale structure at very low redshifts (de Lapparent et al. 1986), consisting of negative density fluctuations on a scale of around 20–50 $h^{-1}\,$Mpc.

4.4. (iv) The assumptions that $\Omega_m = 0.25, \Omega_\Lambda = 0.65$ and $2L_{LSS} = 244 \pm 17\ h^{-1}$ Mpc

Even if the values of the metric parameters are assumed and a scale is chosen, there is no reason why a Poisson noise peak should occur at this particular scale (claimed to be of interest in several observational analyses) in all three redshift intervals, in excess of Poisson noise peaks generated from uncorrelated, random simulations, unless it is cosmological in origin, provided that the simulations mimick any possible peculiar properties of the catalogue.

So, 200 random simulations, using the z-scrambling technique as above, were performed for each redshift interval, for each angular sub-sample, for ($\Omega_{\rm m} = 0.25$, $\Omega_\Lambda = 0.65$).

Similarly to Roukema & Mamon (2001), the probability P_i that a local maximum can occur as close to $2L_{\rm LSS} = 244 \pm 17\,h^{-1}\,$Mpc in the simulation as in the observational catalogue, with at least the same signal-to-noise ratio (Eq. (4)) as the observational local maximum, for the ith redshift interval, is defined

$$P_i \equiv P\Big[\ |r_{\rm sim} - 2L_{\rm LSS}| \le |r_{\rm obs} - 2L_{\rm LSS}| \quad \text{and} \quad (S/N)^{\rm sim} \ge (S/N)^{\rm obs}\ \Big], \tag{18}$$

where the position and signal-to-noise ratio of the first local maximum at $r > r_{\rm min} = 200\,h^{-1}\,$Mpc are $r_{\rm obs}$ and $(S/N)^{\rm obs}$ in the observations and $r_{\rm sim}$ and $(S/N)^{\rm sim}$ in the simulations. The combined probability for the three redshift intervals is

$$P_{123} = P_1 P_2 P_3 \tag{19}$$

since the observational data sets in the three redshift intervals are independent.

The results are $P_1 = P_2 = 0.065, P_3 = 0.075$, so that $P_{123} = 3{\times}10^{-4}$.

In other words, given that ($\Omega_{\rm m} = 0.25, \Omega_\Lambda = 0.65$), the probability that random Poisson signals give a local

maximum as close to $2L_{\rm LSS} = 244\,h^{-1}\,$Mpc as the local maximum in the observational data and of at least as strong a signal-to-noise ratio as the observational local maximum, in all three redshift intervals, is rejected at the 99.97% confidence level.

4.5. Comparison with the analysis of Hoyle et al. (2001)

How do these results compare with the Fourier spectrum analysis by Hoyle et al. (2001)?

Given the large redshift range of the 2QZ–10K (80% of the quasars lie in the range $0.6 \lesssim z \lesssim 2.2$), it is puzzling that Hoyle et al. (2001) found a local maximum to exist for widely differing choices in the local cosmological parameters: it appears to be present both for $(\Omega_{\rm m} = 0.3, \Omega_\Lambda = 0.7)$ and for $(\Omega_{\rm m} = 1.0, \Omega_\Lambda = 0.0)$, at $r \approx 90\,h^{-1}\,$Mpc and $r \approx 65\,h^{-1}\,$Mpc respectively in their analysis.

Comparison of Fig. 8a and Fig. 8b of Hoyle et al. (2001), representing the cases $(\Omega_{\rm m} = 1.0, \Omega_\Lambda = 0.0)$ and $(\Omega_{\rm m} = 0.3, \Omega_\Lambda = 0.7)$ respectively, seems to show a stronger signal in the latter case, but this is still problematic for a feature which should exist at a fixed comoving scale only for the correct values of the local cosmological parameters.

However, differences in the technique of Hoyle et al. (2001) relative to our own include:

(i) Hoyle et al.'s use of a very smooth redshift selection function, which probably does not correct for the selection effects discussed by Scott (1991);
(ii) Hoyle et al.'s inclusion of angular selection regions that have less than 80% "coverage completeness" (two-thirds of their sample lies in regions with only 20%–80% coverage completeness), with a statistical correction for this via their window function;
(iii) use of a Fourier analysis rather than a correlation function;
(iv) use of large, logarithmic bins in k rather than linear bins of $\Delta r = 5\,h^{-1}\,$Mpc in r.

(i) The non-removal of redshift selection effects seems a reasonable candidate for inducing a convolution of an artefact with the real signal, shifting it to the wrong scale, and generating a weak signal for the wrong values of the metric parameters.

(ii) Inclusion of low "coverage completeness" regions is likely to introduce strong sources of noise. Even though this should be statistically corrected by the window function, our own results suggest that it may be more useful simply to ignore low "coverage completeness" regions. The disadvantage is that only about 3000 of the 11 000 quasars can be used, but the advantage is having less noise to correct.

(iii) A Fourier analysis of data with a very complex window function is obviously difficult, and probably more useful for estimating the overall shape of the power spectrum than for the detection of fine features in it. Although in principle, the power spectrum and the correlation function are intrinsically related through Fourier transforms, conversion from one to another is difficult in practice and will be left to other authors, particularly since a large part of the power is removed from our estimate of $\xi(r)$ by the use of z-scrambling: this technique is optimised to detect fine features, not gross features.

It should be noted that in practice, the correlation function is more commonly calculated on small scales, while the power spectrum is calculated on large scales. This is probably because the simplest implementation of calculation of the correlation function, via direct counting of pairs, is more computationally intensive than that of fast Fourier transforms.

However, if $(\Omega_{\rm m}, \Omega_\Lambda)$ parameter space is to be explored, then using correlation functions is more precise than using Fourier transforms. This is because Fourier transforms don't exist in curved space. In curved space over the range considered, calculation of Fourier transforms instead of 3-spherical harmonics or 3-hyperbolic eigenfunctions is still a good approximation up to a few hundred Mpc, since the curvature radius is at least $2860\,h^{-1}\,$Mpc. Moreover, observations indicate that the curvature radius is at least about $10\,000\,h^{-1}\,$Mpc.

(iv) The use of wide, logarithmic bins may make it difficult to detect a feature which (in the present analysis) is much less strong in amplitude than that claimed by Einasto et al. (1997b).

Any or all of these could explain the differences in the two analyses.

It should be noted that Croom et al. (2000) performed a correlation function analysis of the 2QZ–10K on scales below $\sim 100\,h^{-1}\,$Mpc, avoiding problem (iii) above, making calculations to consider the effects of (ii), but retaining problems (i) and (iv). Problem (i) is likely to be insignificant on scales below $\sim 100\,h^{-1}\,$Mpc, so should not be a problem for the purposes of the analysis of Croom et al. (2000).

In this paper, scales above $100\,h^{-1}\,$Mpc are those of most interest, which is why the correction technique of z-scrambling has been used here to avoid problem (i). So, the two studies are complementary and cannot be directly compared.

4.6. Comparison with the analyses of Roukema & Mamon (2000, 2001)

As mentioned above (P. Petitjean, private communication), some fraction of the Iovino et al. (1996) sample of high-quality quasar candidates appears to consist of quasars at wrongly estimated redshifts and stars. This implies that some "redshifts" in the analyses either are those of genuine quasars, but for a misidentifed emission line, or correspond to the emission wavelengths of atomic transitions which should vary little from star to star.

Both cases should add random noise in the cross-correlations, and some genuine correlations should exist

among the misidentified quasars, but at underestimated tangential separations (if the true redshifts are lower than the estimated ones, which is apparently the case).

However, since the emission lines of the stars should be at essentially fixed "false redshifts" (since the velocities of stars are much less than cosmological expansion velocities), the strongest artefact in the sample is likely to be objects at certain favoured "false redshifts".

In this case, the purely tangential analysis (Roukema & Mamon 2000) is likely to be less affected by contaminating objects than the three-dimensional analysis (Roukema & Mamon 2001). Since the scale found in Roukema & Mamon (2000) is consistent with the present value of $L_{\rm LSS} \approx 122 \pm 9\,h^{-1}\,$Mpc for values of $\Omega_{\rm m}$ consistent with those estimated here, the results are compatible.

4.7. Possible theoretical explanations for local maxima in $\xi(r)$

Possible theoretical explanations for fine features in the correlation function or power spectrum include:

(i) acoustic baryonic fluctuations formed during the transition of the recombination epoch, e.g. Eisenstein (1998), Meiksin et al. (1998), Peebles (1999), Miller et al. (1998);
(ii) baryonic fluctuations formed during an inflationary epoch, as a result of the evolution of a complex scalar field condensate, Kirilova & Chizhov (2000);
(iii) phase transitions in supersymmetric models of double inflation, (e.g. Lesgourgues et al. 1998, 2000); or
(iv) string theory inspired fluctuations formed during the Planck epoch. Brandenberger & Martin (2000); Easther et al. (2001).

It would clearly be premature to attempt to distinguish between these on the basis of the 2QZ–10K data.

5. Conclusions

Although considerable care is required to avoid selection effects in the "10K" initial release of the 2dF QSO Redshift Survey (2QZ–10K), it is difficult to avoid the conclusion that a harmonic of the $L_{\rm LSS} \approx 130 \pm 10\,h^{-1}\,$Mpc local maximum in the correlation function or power spectrum of density perturbations, as traced by extragalactic objects, is present in the data and that this scale provides an extremely model-free way of constraining local cosmological parameters without requiring combination with external data sets.

This local maximum was found by estimating the spatial two-point autocorrelation functions $\xi(r)$ of the three-dimensional (comoving, spatial) distribution of the $N = 2378$ quasars in the most completely observed ($\geq$85% spectroscopic completeness) and "covered" ($\geq$80% coverage completeness) sky regions of the catalogue, over the redshift ranges $0.6 < z < 1.1$ ("low-z"), $1.1 < z < 1.6$ ("med-z"), and $1.6 < z < 2.2$ ("hi-z"), using the z-scrambling technique in order to avoid selection effects.

(i) Avoiding a priori estimates of the length scales of features, local maxima in $\xi(r)$ are found in the different redshift ranges. The requirement that a local maximum be present in all three redshift ranges at the same comoving length scales implies strong, purely geometric constraints on the local cosmological parameters. The only local maximum satisfying this requirement is that at a length scale of $2L_{\rm LSS} = 244 \pm 17\,h^{-1}\,$Mpc.
(ii) For a standard cosmological constant FLRW model, the matter density and cosmological constant are constrained to $\Omega_{\rm m} = 0.25 \pm 0.10, \Omega_\Lambda = 0.65 \pm 0.25$ (68% confidence), $\Omega_{\rm m} = 0.25 \pm 0.15, \Omega_\Lambda = 0.60 \pm 0.35$ (95% confidence), respectively, *from the 2QZ–10K alone*.
(iii) For an effective quintessence ($w_{\rm Q}$) model and zero curvature, $w_{\rm Q} < -0.5$ (68% confidence), $w_{\rm Q} < -0.35$ (95% confidence) are found, again *from the 2QZ–10K alone*.

These results are consistent with type Ia supernovae and microwave background results (e.g. Perlmutter et al. 1999; Riess et al. 1998; Lange et al. 2000; Balbi et al. 2000), but avoid the need to combine two data sets in order to obtain constraints on both $\Omega_{\rm m}$ and Ω_Λ.

The constraints on $\Omega_{\rm m}$ are, of course, in remarkable agreement with the constraints from kinematics of galaxy clusters (e.g. Carlberg et al. 1997), collapsing galaxy groups (Mamon 1993), as well as from the baryonic fraction in clusters (White et al. 1993; Mohr et al. 1999) and groups (Henriksen & Mamon 1994).

However, in contrast to Jaffe et al. (2000), who exclude a flat universe at about ~95% significance, i.e. $\Omega_{\rm m} + \Omega_\Lambda = 1.11^{+0.13}_{-0.12}$ at 95% confidence, a hyperbolic universe is weakly favoured here, though a flat universe is consistent with the data at the 68% confidence level.

The present results also contrast with the constraint from the quietness of the Hubble flow (Chemin 2000 and Sect. 5 of Sandage 1999) which requires a cosmological constant of about $\Omega_\Lambda = 0.8$ or higher.

It should be emphasised that the 2QZ–10K data establish the existence of a non-zero cosmological constant independently of the supernovae results: $\Omega_\Lambda = 0$ is refuted at the 99.7% confidence level.

The full 2QZ will clearly provide even more impressive constraints on local maxima, $\Omega_{\rm m}$, Ω_Λ and $w_{\rm Q}$.

Acknowledgements. Useful comments from Patrick Petitjean, Brian Boyle and Scott Croom are gratefully acknowledged. The 2QZ–10K was based on observations made with the Anglo-Australian Telescope and the UK Schmidt Telescope. Use of the resources at the Centre de Données astronomiques de Strasbourg (`http://csdweb.u-strasbg.fr`), the support of the Institut d'Astrophysique de Paris, CNRS, for a visit during which part of this work was carried out, and the support of la Société de Secours des Amis des Sciences are gratefully acknowledged. This research has been supported by the Polish Council for Scientific Research Grant KBN 2 P03D 017 19 and has benefited from the Programme jumelage 16 astronomie

France/Pologne (CNRS/PAN) of the Ministère de la recherche et de la technologie (France).

References

Adelberger, K. L., Steidel, C. C., Giavalisco, M., et al. 1998, ApJ, 508, 18, 1998

Arnouts, S., Cristiani, S., Moscardini, L., et al. 1999, MNRAS, 310, 540

Balbi, A., et al. (Maxima collaboration) 2000, ApJ, 545, L1 [astro-ph/0005124]

Baugh, C. M., & Efstathiou, G. 1993, MNRAS, 265, 145,

Baugh, C. M., & Efstathiou, G. 1994, MNRAS, 267, 323

Boyle, B. J., Shanks, T., Croom, S. M., et al. 2000, MNRAS, in press [astro-ph/0005368]

Broadhurst, T. 1999, in Clustering at High Redshift, ed. V. Le Brun, A. Mazure, & O. Le Fèvre, in press

Broadhurst, T. J., Ellis, R. S., Koo, D. C., & Szalay, A. S. 1990, Nature, 343, 726

Broadhurst, T., & Jaffe, A. H. 1999, submitted [astro-ph/9904348]

Carlberg, R. G., Yee, H. K. C., & Ellingson, E. 1997, ApJ, 478, 462

Chemin, A. 2000, Adv. Sp. Res., submitted

Croom, S. M., Shanks, T., Boyle, B. J., et al. 2000, MNRAS [astro-ph/0012375]

Croom, S. M., Smith, R. J., Boyle, B. J., et al. 2001, MNRAS, 322, L29

da Costa, L. N. 1992, in The Distribution of Matter in the Universe, ed. G. A. Mamon, & D. Gerbal (Meudon: Obs. de Paris), 163 ftp://ftp.iap.fr/pub/from_users/gam/PAPERS/DAECMTG/dacosta.dvi.Z

da Costa, L. N., et al. 1993, in Cosmic Velocity Fields, ed. F. Bouchet, & M. Lachièze-Rey (Gif-sur-Yvette, France: Éditions Frontières), 475

de Lapparent, V., Geller, M. J., & Huchra, J. P. 1986, ApJ, 302, L1

de Lapparent, V., Geller, M. J., & Huchra, J. P. 1991, ApJ, 369, 273

Deng, Z., Xiaoyang, X., & Fang, L.-Zh. 1994, ApJ, 431, 506

Deng, X.-F., Deng, Z.-G., & Xia, X.-Y. 1996, Chin. Astron. Astroph., 20, 383

Easther, R., Greene, B. R., Kinney, W. H., & Shiu, G. 2001 [hep-th/0104102]

Efstathiou, G. 1999, MNRAS, 310, 842

Einasto, M., Einasto, J., Tago, E., Dalton, G. B., & Andernach, H. 1994, MNRAS, 269, 301

Einasto, J., Einasto, M., Frisch, P., et al. 1997, MNRAS, 289, 801

Einasto, J., Einasto, M., Gottloeber, S., et al. 1997, Nature, 385, 139

Eisenstein, D. J., Hu, W., Silk, J., & Szalay, A. S. 1998, ApJ, 494, L1

Gaztañaga, E., & Baugh, C. M. 1998, MNRAS, 294, 229

Geller, M. J., & Huchra, J. P. 1989, Science, 246, 897

Groth, E. J., & Peebles, P. J. E. 1997, ApJ, 217, 385

Guzzo, L. 1999, in proceedings of XIX Texas Symp. Rel. Astr. [astro-ph/9911115]

Henriksen, M. J., & Mamon, G. A. 1994, ApJ, 421, L63

Hoyle, F., Outram, P. J., Shanks, T., et al. 2001, MNRAS, submitted [astro-ph/0102163]

Iovino, A., Clowes, R., & Shaver, P. 1996, A&AS, 119, 265

Jaffe, A. H., et al. 2000 [astro-ph/0007333]

Kirilova, D. P., & Chizhov, M. V. 2000, MNRAS, 314, 256

Landy, S. D., & Szalay, A. S. 1993, ApJ, 412, 64

Lange, A. E., et al. (Boomerang collaboration) 2000 [astro-ph/0005004]

Lesgourgues, J. 2000, Nucl. Phys. B, 582, 593 [hep-ph/9911447]

Lesgourgues, J., Polarski, D., & Starobinsky, A. A. 1998, MNRAS, 297, 769

Luminet, J.-P., & Roukema, B. F. 1999, in Theoretical and Observational Cosmology, NATO Advanced Study Institute, Cargèse 1998, ed. M. Lachièze-Rey (Netherlands: Kluwer), 117 [astro-ph/9901364]

Mamon, G. A. 1993, in The N-Body problem & Gravitational Dynamics, ed. F. Combes, & E. Athanassoula (Meudon: Obs. Paris), 188 [astro-ph/9308032]

Brandenberger, R. H., & Martin, J. 2000, [astro-ph/0005432]

Meiksin, A., White, M., & Peacock, J. A. 1999, MNRAS, 304, 851

Miller, C. J., Nichol, R. C., & Batuski, D. J. 2001, Science, 292, 2302

Mohr, J. J., Mathiesen, B., & Evrard, A. E. 1999, ApJ, 517, 627

Osmer, P. S. 1981, ApJ, 247, 762

Peebles, P. J. E. 1999, ApJ, 510, 531

Perlmutter, S., Aldering, G., Goldhaber, G., et al. 1999, ApJ, 517, 565

Riess, A. G., Filippenko, A. V., Challis, P., et al. 1998, AJ, 116, 1009

Roukema, B. F. 2000, Bull. Ast. Soc. India, 28, 483

Roukema, B. F. 2001, MNRAS, 325, 138

Roukema, B. F., & Mamon, G. A. 2000, A&A, 358, 395

Roukema, B. F., & Mamon, G. A. 2001, A&A, 366, 1

Roukema, B. F., Valls-Gabaud, D., Mobasher, B., & Bajtlik, S. 1999, MNRAS, 305, 151

Sandage, A. 1999, ApJ, 527, 479

Scott, D. 1991, A&A, 242, 1

Shanks, T., Boyle, B. J., Croom, S. M., et al. 2000, in Clustering at High Redshift, ed. A. Mazure, O. Le Fèvre, & V. Lebrun, ASP [astro-ph/0003206]

Smith, R. J., Boyle, B. J., Shanks, T., et al. 1998, in IAU Symp. 179 New Horizons from Multi-Wavelength Sky Surveys, ed. B. J. McLean, D. A. Golombek, J. J. E. Hayes, & H. E. Payne (Kluwer), 348

Tadros, H., & Efstathiou, G. 1996, MNRAS, 282, 1381

Tago, E., Einasto, J., Einasto, M., Müller, V., & Andernach, H. 2001, AJ, submitted [astro-ph/0012537]

Tucker, D. L., Lin, H., & Shectman, S. 1972, in Wide Field Surveys in Cosmology, ed. S. Colombi, Y. Mellier, B. Raban, & S. Weinberg, Gravitation and Cosmology (New York, USA: Wiley)

White, S. D. M., Navarro, J. S., Evrard, A. E., & Frenk, C. S. 1993, Nature, 366, 429